U. S. DEPARTMENT OF COMMERCE
NATIONAL OCEANIC AND ATMOSPHERIC ADMINISTRATION
NATIONAL WEATHER SERVICE
NATIONAL METEOROLOGICAL CENTER

OFFICE NOTE 83

Noise Suppression in the Eight-Layer Global Model

R. D. McPherson
J. D. Stackpole
Development Division

MAY 1973

NOISE SUPPRESSION IN THE EIGHT-LAYER GLOBAL MODEL

I. Introduction

The examination of unwanted "noise" oscillations in primitive-equations models is an area of enquiry to be approached with great reluctance and only by those of stout heart and strong stomach. If caution and a sense of perspective are not maintained, the investigator may be seduced into concluding that abandoning the quasi-geostrophic equations for the primitive form was a colossal blunder. It is often the case that the noise components exhibit sufficiently large amplitudes that the essential goodness of the prediction of motions of meteorological interest is obscured; yet these components can frequently be suppressed by judicious use of any of a number of numerical devices.

This note reports on a preliminary and somewhat subjective investigation of the principal noise components present in the NMC eight-layer global model (Stackpole, Vanderman, and Shuman, 1973), and on a series of experiments designed to reduce the amplitudes of these components. Our motivation has been in part a concern for the numerical stability of medium-range integrations of the model, and in part due to the intended use of the global model in conjunction with Flattery's* global spectral analysis method as an operational four-dimensional data assimilation system (McPherson and Bonner, 1972). For the latter purpose, the analysis-forecast system will be employed in a series of forecasts with reanalysis each six hours using the six-hour forecast as a first guess. It is important that these forecasts be as free from noise as possible.

II. Noise in the Global Model

For the purposes of this note, we have chosen to examine the characteristics of the noise in only a few, largely subjective, ways. In Figure 1, the behavior of three pressure variables, the surface pressure, the tropopause pressure, and the pressure thickness of the so-called thetasphere, are displayed as predicted by the global model at hourly intervals for an individual grid point. Inspection of the surface pressure trace reveals an oscillation with a period of 3-4 hours and an amplitude of 2-3 mb. A longer-period oscillation is evident in the tropopause pressure, superimposed on a presumably meteorological trend. The period is approximately 5-6 hours, and the amplitude is again 2-3 mb.

---

*promised manuscript

The heights of the 1000 mb, 500 mb, and 300 mb surfaces for the same grid point are plotted in Figure 2. An oscillation with a 3-hour period is present, as in the surface pressure trace. Its amplitude is approximately 10-15 meters and is in phase at all levels. We may, therefore, conclude that this represents an external gravity wave. The longer-period oscillation noted in the tropopause pressure is not apparent, at least by visual inspection. One point worth noting is that the height changes in the first hour of about 40 meters at all levels are another indication that the initial balance inherent in the global spectral analysis system is not completely compatible with the prediction model.

The presence of these gravitational oscillations in the prediction is also reflected in the graphs of global mean-square divergence shown in Figure 3. Total mean-square divergence for all layers of the model is the quantity displayed. The total mean-square divergence increases by nearly an order of magnitude over the 12-hour period. This behavior is a source of concern for the numerical stability of the model in medium- and extended-range integrations.

The oscillations apparent in Figures 1 and 2 are nonmeteorological in character, and their amplitudes are not insignificant. Their presence detracts from the accuracy of the forecasts of meteorological features. We believe that the resulting inaccuracy becomes especially important when the model is employed in a series of short-period forecasts for data assimilation. Therefore, an effort to reduce the noise is warranted.

One approach to this problem would be to adjust the initial mass and motion fields to minimize the imbalance which generates the noise; this is the initialization problem. Another approach is to damp the oscillations during the course of the integration. It is likely that an adequate solution to the problem will ultimately involve both approaches. However, in this note we examine only a device belonging to the latter approach. The next two sections describe its formulation and testing.

III. Numerical Formulation of the Divergence Damper

Several years ago, Shuman and Stackpole (1969) suggested special viscosity terms which can be made to damp either the rotational or the divergent component of the wind. This topic was subsequently taken up again by Shuman (1969). It was not a new idea: Lamb (1932) discusses the damping of the rotational component of the wind with this device. Quite recently, French investigators (Morel and Talagrand, 1972; Sadourny, 1972) have suggested the use of the divergence-damping viscosity term as an attractive alternative to the Euler-backward method for damping the gravitational "shocks" produced by continuous four-dimensional data assimilation.

One may express the equations of motion as

$$\frac{\partial u}{\partial t} + \cdots - \mu\frac{\partial D}{\partial x} + \nu\frac{\partial \zeta}{\partial y} = 0 \qquad (1)$$

$$\frac{\partial v}{\partial t} + \cdots - \mu\frac{\partial D}{\partial y} - \nu\frac{\partial \zeta}{\partial x} = 0 \tag{2}$$

where D and ζ represent divergence and vorticity, respectively.

Forming the divergence and vorticity equations from (1) and (2), we obtain

$$\frac{\partial D}{\partial t} + \cdots - \mu\nabla^2 D = 0 \tag{3}$$

$$\frac{\partial \zeta}{\partial t} + \cdots - \nu\nabla^2 \zeta = 0 \tag{4}$$

Shuman (1969) points out that with $\nu=0$, gravitational oscillations may be damped without directly affecting the vorticity. We will henceforth denote the viscous terms in (1) and (2) with $\nu=0$, $\mu\neq 0$ as the "divergence damper." Its numerical formulation in spherical geometry will next be considered.

Consider the simple differential equations in spherical coordinates (λ,ϕ, r),

$$\frac{\partial u}{\partial t} = \frac{\mu}{r\cos\phi}\frac{\partial D}{\partial \lambda} \tag{5}$$

and

$$\frac{\partial v}{\partial t} = \frac{\mu}{r}\frac{\partial D}{\partial \phi} \tag{6}$$

where the divergence D is defined as

$$D \equiv \frac{1}{r\cos\phi}\left\{\frac{\partial u}{\partial \lambda} + \frac{\partial}{\partial \phi}(v\cos\phi)\right\} \tag{7}$$

Now consider the finite-difference analogue. Assume for simplicity that u and v are defined at the grid points in the schematic below, and the divergence is defined at

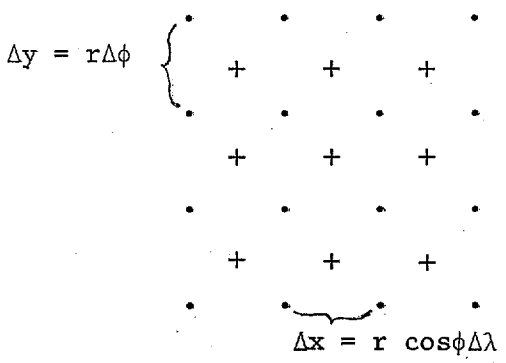

the centers of grid squares marked by crosses. We will make use of the following averaging and differencing operators:

$$F_x = \frac{F_{i+\frac{1}{2}} - F_{i-\frac{1}{2}}}{r\cos\phi\left(\lambda_{i+\frac{1}{2}} - \lambda_{i-\frac{1}{2}}\right)} = \frac{F_{i+\frac{1}{2}} - F_{i-\frac{1}{2}}}{\Delta x} \tag{8}$$

$$\overline{F}^x = \tfrac{1}{2}\left[F_{i+\frac{1}{2}} + F_{i-\frac{1}{2}}\right]. \tag{9}$$

$$F_y = \frac{F_{j+\frac{1}{2}} - F_{j-\frac{1}{2}}}{r\left(\phi_{j+\frac{1}{2}} - \phi_{j-\frac{1}{2}}\right)} = \frac{F_{j+\frac{1}{2}} - F_{j-\frac{1}{2}}}{\Delta y} \tag{10}$$

$$\overline{F}^y = \tfrac{1}{2}\left(F_{j+\frac{1}{2}} - F_{j-\frac{1}{2}}\right) \tag{11}$$

It is convenient to expand (7) before applying finite differences:

$$D = \frac{1}{r\cos\phi}\frac{\partial u}{\partial\lambda} + \frac{1}{r}\frac{\partial v}{\partial\phi} - \frac{v}{r}\tan\phi \tag{12}$$

or, if we define

$$\partial x \equiv r\cos\phi\,\partial\lambda \tag{13}$$

$$\partial y \equiv r\,\partial\phi, \tag{14}$$

ignoring the obvious sloppiness in mathematical notation, then (12) becomes

$$D = \frac{\partial u}{\partial x} + \frac{\partial v}{\partial y} - \frac{v}{r}\tan\phi \tag{15}$$

In finite difference form, this becomes

$$D = \overline{u}^{y}_{x} + \overline{v}^{x}_{y} - \overline{\frac{\overline{v}^{y}}{r}\tan\phi}^{x}, \tag{16}$$

which produces divergence in the centers of grid squares from wind components defined at points. The finite difference forms of (5) and (6) become

$$\overline{u}^{t}_{t} = \mu\,\overline{D}^{y}_{x} \tag{17}$$

and

$$\overline{v}^{t}_{t} = \mu\,\overline{D}^{x}_{y} \tag{18}$$

which yields wind tendencies at grid points from divergences in grid cells. This is contrary to the situation which exists in the eight-layer global model.

We propose to take care of this difficulty by redefining the divergence. In particular, we will define a grid-point estimate of divergence D* by

$$D^* \equiv \overline{D^{xy}}^{xy} = \left(\overline{u_x}^{y}{}^{x} + \overline{v_y}^{x}{}^{y} - \overline{\frac{v}{r}\tan\phi}^{y}{}^{x} \right)^{xy} . \tag{19}$$

Eqns. (17) and (18) then become

$$\overline{u}^{t}_{t} = \mu \overline{D^*}^{y}_{x} \tag{20}$$

$$\overline{v}^{t}_{t} = \mu \overline{D^*}^{x}_{y} , \tag{21}$$

which yields winds in grid cells from divergence estimates at grid points. Unfortunately, this form suffers from a defect pointed out by Shuman (1969) in connection with the earlier work of Shuman and Stackpole: *the shortest resolvable waves are not affected by the divergence damper.* This is due primarily to the use of a "coupled grid lattice" (see NMC Office Note 32, and Robert, Shuman, and Gerrity, 1970) in constructing the model. Although experiments have been made with other 'decoupled' lattice structures, no completely satisfactory alternativesis yet ready for operational implementation. Until such an alternative is available, it seems prudent to employ the divergence damper against those wavelengths for which it is effective, and rely on other devices, such as external filters or spectral truncation, to handle the shortest waves.

We next present the results of several experiments with the global model and the divergence damper.

IV. Experimental Results

In order to determine the effectiveness of the divergence damper for controlling gravitational oscillations, several integrations of the global model were performed. All utilized the same initial, global analyses for 00Z, February 5, 1973, provided by Flattery's spectral analysis method. The choice of the appropriate value of the viscosity coefficient μ was guided by the suggestion of Morel and Talagrand (1972) of $\mu = 10^8 m^2 sec^{-1}$. We regarded this large value as the maximum to be used. The experiments, and their principal characteristics with respect to the divergence damper, are listed in Table 1.

Table 1

Experiment	$\mu (m^2 sec^{-1})$	Other characteristics
1	10^7	12-hour forecast
2	10^8	" " "
3	0	" " "
4	0	Euler-backward for 12 hrs.
5	10^8 for first 2 hours, then 10^7 for 10 hours	
6	2.5×10^7	12-hour forecast
7	5×10^7	" " "
8	7.5×10^7	" " "

Thus, six 12-hour integrations were carried out with $10^7 \leq \mu \leq 10^8$. For comparison, one 12-hour forecast was performed with $\mu = 0$ and no damping except for a time filter* to control the temporal computational mode, and one 12-hour forecast with $\mu = 0$, but using the Euler-backward damping time-integration scheme.

Figure 5 displays the total global mean-square divergence as a function of time, for each of the eight integrations. The solid line represents experiment 3, the same curve as Figure 3. With regard to the six experiments involving nonzero values of μ, it will be seen that the minimum value used, $\mu = 10^7 m^2 sec^{-1}$ in experiment 1, allowed a growth of mean-square divergence during the first six hours. After the seventh hour, it levels off to reach a final value approximately half that of the $\mu = 0$ case.

There is little difference in the behavior of mean-square divergence for $5 \times 10^7 \leq \mu \leq 10^8$. It is interesting to note the result of experiment

*See Asselin (1972), and Gerrity and Scolnik (1971); the filter in this case effectively weights the τ-1, τ, and τ+1 values by $\frac{1}{4}$, $\frac{1}{2}$, $\frac{1}{4}$ respectively.

5, in which $\mu = 10^8 m^2 sec^{-1}$ for the first two hours, and then $\mu = 10^7 m^2 sec^{-1}$ for the remaining ten hours. The trace follows exactly that of experiment 2 ($\mu = 10^8$) for the first two hours, but then rises abruptly and becomes coincident with the experiment 1 trace ($\mu = 10^7$) after the ninth hour. This suggests that the cumulative effect of the divergence damper is not great during the initial adjustment; the model evidently has a short memory.

Finally, it is worth noting the mean-square divergence trace produced from experiment 4, which used another popular damping device, the Euler-backward time-integration method. The damping of divergence by this method is both slower and not as effective in reducing the growth rate.

From examination of only the mean-square divergence, then, it may be concluded that the divergence damper with $10^7 \leq \mu \leq 10^8$ is far more effective in reducing the growth of divergence than is the Euler-backward. Fortunately, it is also much cheaper. However, since the "plateau" value of divergence most compatible with the meteorological flow is not known, the choice of the proper value of μ must be made from other considerations.

One such consideration must be the ability to damp the oscillations evident in Figures 1 and 2. Figure 6 displays the same pressure variables as in Figure 1, for $\mu = 0$, 1×10^7, 2.5×10^7, and $1 \times 10^8 m^2 sec^{-1}$. Damping associated with the smallest nonzero value of μ is negligible. The shortest-period oscillation is affected most, but the reduction in amplitude is very small. At the other extreme, $\mu = 10^8 m^2 sec^{-1}$ is extremely effective in damping both the short- and intermediate-period oscillation. As might be expected, the damping produced by $\mu = 2.5 \times 10^7 m^2 sec^{-1}$ lies between the extreme (nonzero) values. However, only the maximum value of μ appreciably damps the longest-period oscillation, and the extent of that damping is obscured by another effect which will be discussed presently.

A similar result is apparent in Figure 7, showing 1000 mb, 500 mb, and 300 mb heights, as in Figure 2, for the same values of μ as in Figure 6. There are, however, some additional points of interest. First, the value $2.5 \times 10^7 m^2 sec^{-1}$ appears somewhat more effective against the 3-hour oscillation in height field than is the case in the surface pressure. Secondly, the damping of the longest-period oscillation is not so apparent with $\mu = 10^8 m^2 sec^{-1}$. Also, this value results in a change of 46 m at 1000 mb at the 12th hour over the $\mu = 0$ case. The magnitude of this change is distressingly large, although it is interesting that it decreases with height.

It is therefore evident that the divergence-damper does indeed damp divergence, and is effective against gravitational oscillations, especially those of higher frequency. We now examine the effect of this device on the large-scale meteorological fields. Figures 8, 9, and 10 show the initial sea-level pressure, 500 mb height, and mean relative humidity displayed on a polar stereographic projection of the Northern Hemisphere. Attention

should be directed particularly at the principal areas of irregular terrain, western North America and south-central Asia. Figures 11, 12, and 13 show 12-hour forecasts for these same fields from the case in which $\mu = 0$.

There is nothing especially remarkable about these forecasts; they are included only for comparison with the corresponding charts from the $\mu = 10^8 m^2 sec^{-1}$ shown in Figures 14, 15, and 16. Comparing Figure 14 with Figure 11, the most striking difference is that the larger value of μ has amplified the flow pattern in the vicinity of markedly irregular terrain. In Asia, North America, and Greenland, high pressures over and upstream from the principal mountain barriers have been increased and the lee troughs intensified. This same tendency is apparent at the 500 mb level as well, as indicated in Figures 12 and 15. Particularly distressing is the significant cross-contour flow of the winds in the vicinity of the steeply-sloping terrain. Figures 17 and 18 display the differences between the two surface and two 500 mb forecasts.

The divergence-damper thus makes the model "feel" the underlying terrain to an undue degree. We speculate, in the absence of convincing evidence, that this behavior is related to the fact that in the vicinity of steeply-sloping terrain, the winds in the sigma-coordinate system are not horizontal--but include a substantial vertical (geometric) component as well. Terms such as the divergence damper are therefore not exclusively lateral viscosity terms, but represent vertical mixing also. This may not be completely undesirable, but it is evident that care must be taken to avoid excessively large values of μ.

It may be noted at this point that the noticeable increase in pressures and heights with $\mu = 10^8 m^2 sec^{-1}$ at the point shown in Figures 6 and 7 is undoubtedly a reflection of the presence of the Andes barrier a short distance downstream.

Another damaging side-effect of the divergence damper with large viscosity coefficients may be seen in a comparison of Figures 13 and 16, showing the 12-hour forecasts of mean relative humidity. In general, $\mu = 10^8 m^2 sec^{-1}$ results in a diminution of the relative humidity maxima; there are no 90 percent centers in Figure 16. One consequence of this is a drastic reduction of precipitation predicted by the model.

Table 2 presents a summary of the differences between the case of $\mu = 0$ and the remaining experiments. On the evidence given in the Table and in preceding paragraphs, it appears that $\mu = 10^8 m^2 sec^{-1}$ is too large, while $\mu = 10^7 m^2 sec^{-1}$ is too small to effectively damp the short-period oscillations. An appropriate intermediate value seems to be $2.5 \times 10^7 m^2 sec^{-1}$. This value controls the growth of mean-square divergence, as demonstrated in Figure 5, and is fairly effective against the 3-hour and 6-hour oscillations from Figures 6 and 7.

Table 2

Differences between experiments with $\mu = 0$ (experiment 3) and other experiments. Given are global means and mean-square measures of sea-level pressure, 500 mb height, 300 mb height, and 1000-500 mb thickness.

Experiment character	SLP		Z_{500}		Z_{300}		$H_{1000-500}$	
	Mean (mb)	Mean-square $(mb)^2$	Mean (m)	Mean-square (m^2)	Mean (m)	Mean-square (m^2)	Mean (m)	Mean-square (m^2)
1. 10^7	-.0003	0.38	0.530	20.2	1.45	30.1	0.52	12.6
2. 10^8	-.0674	9.90	-0.491	510.5	2.46	576.5	0.04	166.8
4. Euler-backward	.0102	0.98	0.289	67.5	0.40	69.3	0.08	3.0
5. 10^8 then 10^7	-.0741	0.91	-0.418	56.1	0.55	65.4	0.21	18.4
6. 2.5×10^7	-.0167	1.69	0.152	84.3	1.80	109.0	0.28	42.6
7. 5×10^7	-.0364	4.23	-0.123	207.1	2.28	225?9	.016	91.3
8. 7.5×10^7	-.0470	6.87	-.231	343.4	2.52	404.6	0.13	132.4

Figures 19, 20, and 21 represent the 12-hour forecasts from the case of $\mu = 2.5 \times 10^7 m^2 sec^{-1}$, and Figures 22 and 23 show the difference in sea-level pressure and 500 mb height between this case and $\mu = 0$. The flow pattern is not greatly disturbed, and the differences near the mountains are much smaller than for $\mu = 10^8 m^2 sec^{-1}$. However, Figure 21 indicates that the mean relative humidity is diminished in the maxima, as was the case for $\mu = 10^8 m^2 sec^{-1}$.

V. Conclusions

The following tentative conclusions may be drawn:

1. The divergence damper is an effective numerical stability device;

2. It does reduce the amplitude of short-period (3-6 hours) gravitational oscillations.

3. Its effectiveness is very sensitive to the chosen value of the viscosity coefficient in the range $10^7 \leq \mu \leq 10^8 m^2 sec^{-1}$.

4. Its use, with $\mu \geq 2.5 \times 10^7 m^2 sec^{-1}$, entails very disagreeable side-effects, including excessive amplification of the influence of mountain barriers and reduction of precipitation; the latter effect is also evident to some degree, even for $\mu < 2.5 \times 10^7 m^2 sec^{-1}$.

On balance, the divergence damper with $\mu = 2.5 \times 10^7 m^2 sec^{-1}$ will produce adequate damping of the short-period noise, with a minimum of undesirable side effects except that the reduction of precipitation may still be unacceptable. In view of this, it may be desirable to employ this value for the first several hours, and then reduce it.

Even so, the use of the divergence damper with $\mu = 2.5 \times 10^7 m^2 sec^{-1}$ does not appear to affect appreciably the relatively long-period ($\approx$10 hours) oscillation, nor does it cure the initial "shock" evident in the large first-hour changes shown in Figures 6 and 7. The noise problem is therefore not solved, and attention must now focus on appropriate initialization procedures to improve the initial balance.

References

Asselin, R., 1972: "A frequency filter for time integrations," Monthly Weather Review, Vol. 100, No. 6.

Gerrity, J., and S. Scolnik, 1971: "Some comments on Robert's time filter for time integration," NMC Office Note 62.

Lamb, H., 1932: Hydrodynamics, London, Cambridge University Press.

McPherson, R., and W. Bonner, 1972: "Toward an operational four-dimensional data assimilation system," NMC Office Note 80.

Morel, P., and O. Talagrand, 1972: "The dynamic approach to meteorological data assimilation," unpublished manuscript, Laboratoire de Météorologie Dynamique, Ecole Normale Superieure, Paris.

Robert, A., F. Shuman, and J. Gerrity, 1970: "On partial difference equations in mathematical physics," Monthly Weather Review, Vol. 98, No. 1.

Sadourny, R., 1972: "Forced geostrophic adjustment in large-scale flow," Laboratoire de Météorologie Dynamique du C.N.R.S., Paris, unpublished manuscript.

Shuman, F., 1969: "On a special form for viscous terms," NMC Office Note 32.

Shuman, F., and J. Stackpole, 1969: "The currently operational NMC model, and results of a recent numerical experiment," Proc. WMO/IUGG Symp. NWP, Tokyo, Japan Meteorological Agency, II-55-98.

Stackpole, J., L. Vanderman, and F. Shuman, 1973: "The NMC 8-layer global Primitive equation model on a latitude-longitude grid," to be published in the GARP series.

List of Figures

Figures (continued)

14. Same as Figure 12, for experiment 2.

15. Same as Figure 13, for experiment 2.

16. Difference between 12-hr forecasts of sea level pressure from experiments 3 and 2 (Exp. 3-- Exp. 2), at intervals of 4mb.

17. Difference between 12-hr forecasts of 500 mb height from experiments 3 and 2, at intervals of 30m.

18. Same as Figure 11, for experiment 6.

19. Same as Figure 11, for experiment 6.

20. Same as Figure 11, for experiment 6.

21. Same as Figure 17, except experiment 3 - experiment 6.

22. Same as Figure 18, except experiment 3 - experiment 6.

POINT 15N, 40S

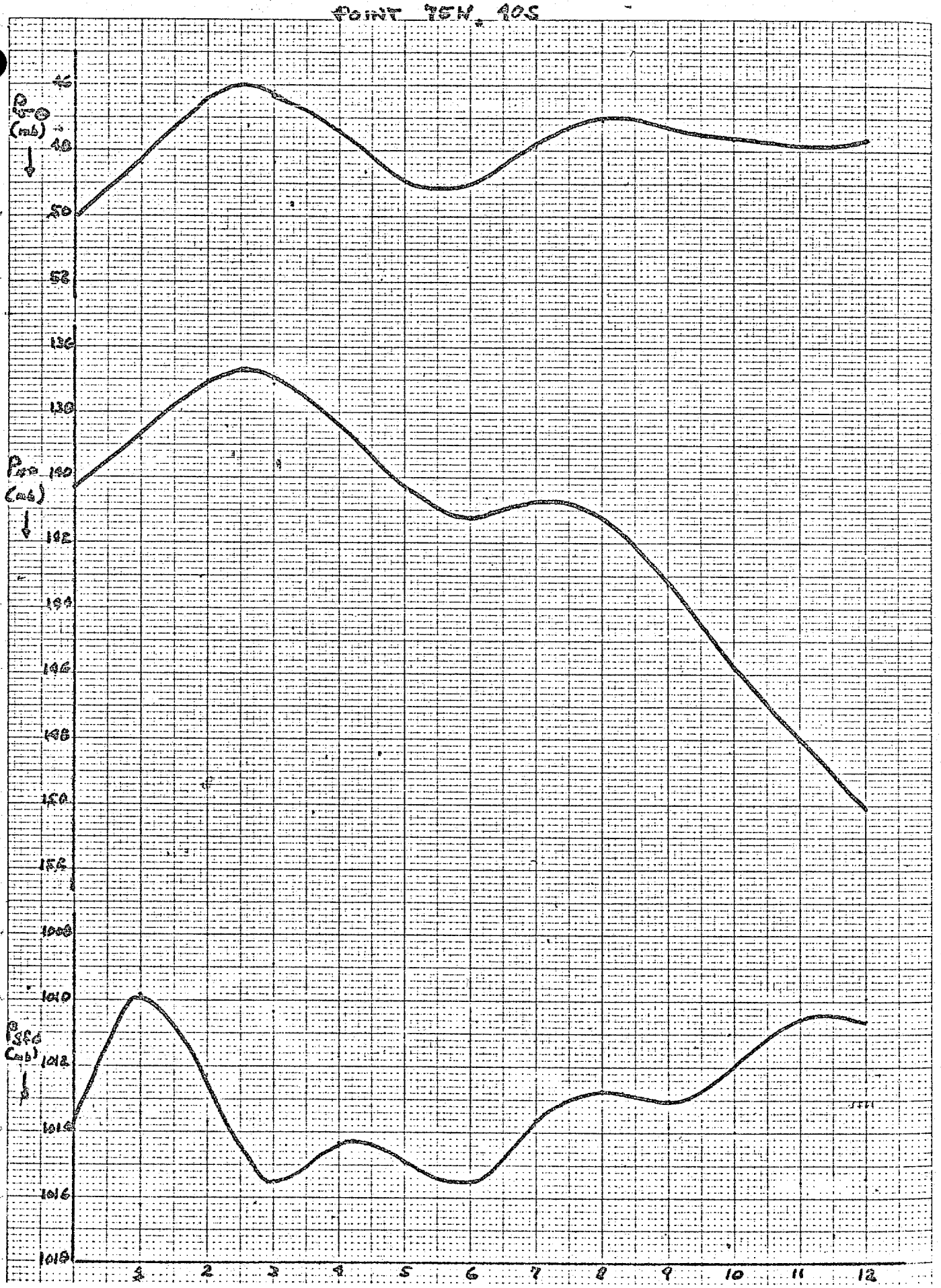

Point 75W, 40S

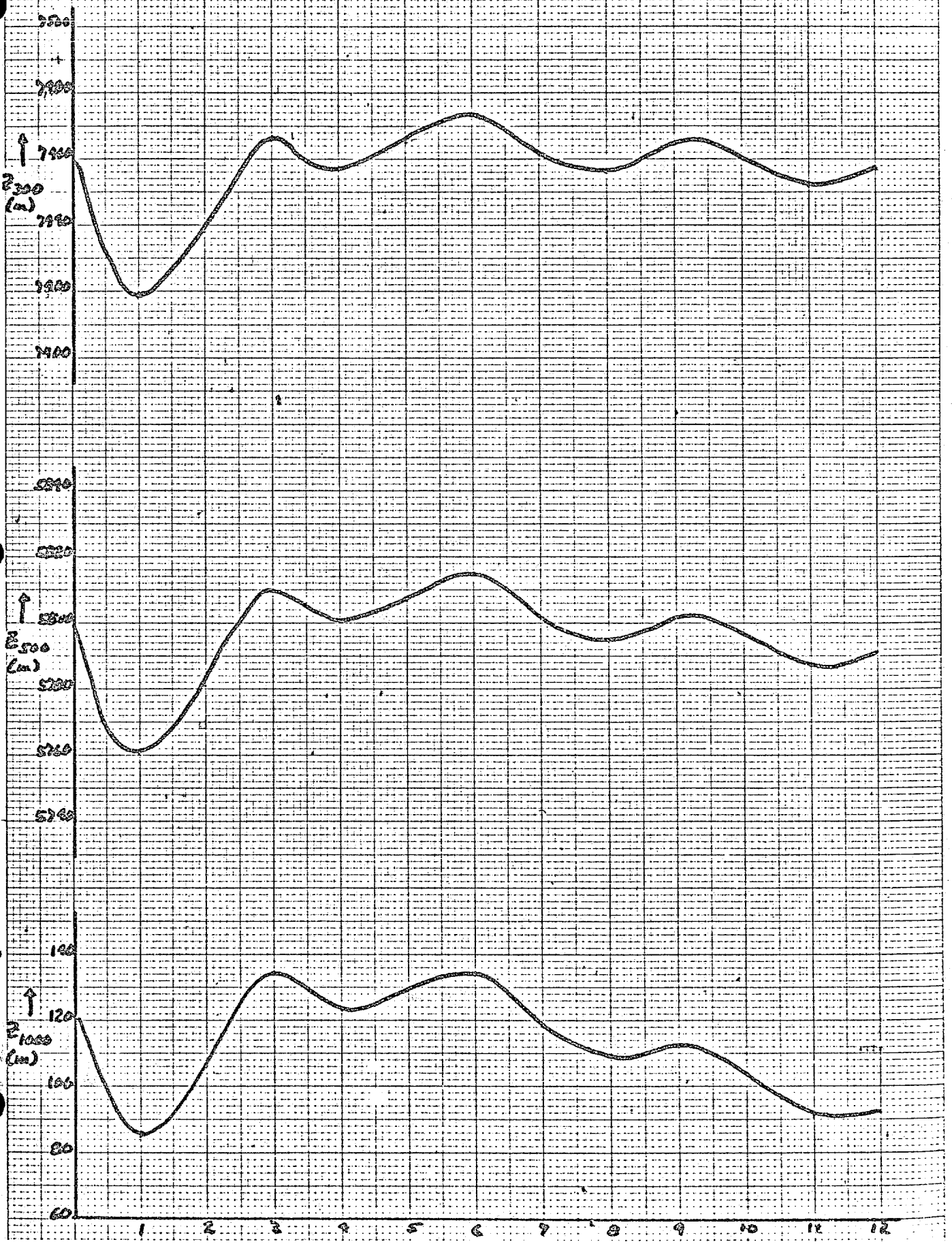

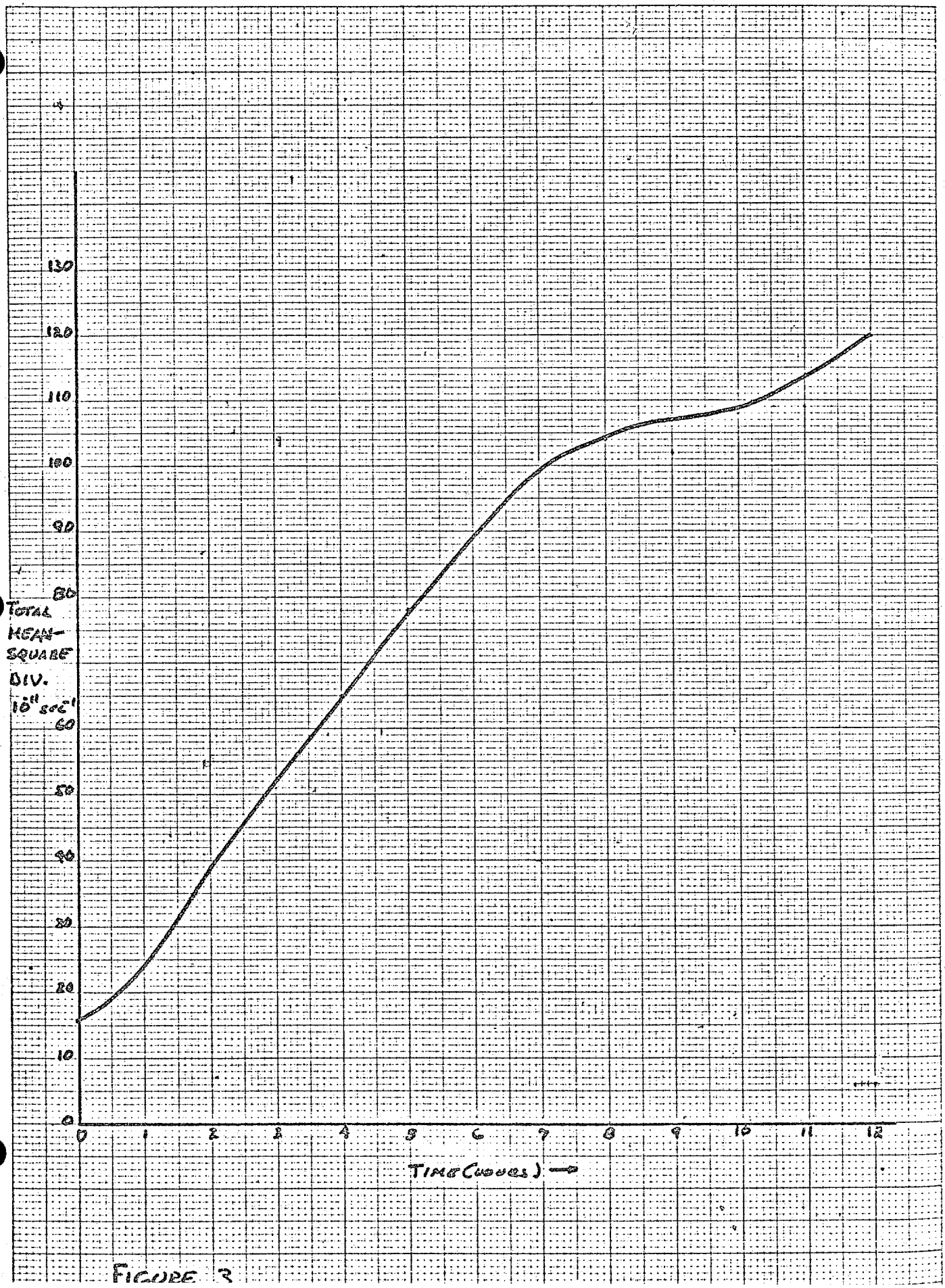
130
120
110
100
90
80
TOTAL MEAN-SQUARE DIV. 10^{11} sec^{-1}
60
50
40
30
20
10
0
0
1
2
3
4
5
6
7
8
9
10
11
12
TIME (HOURS) →

FIGURE 3

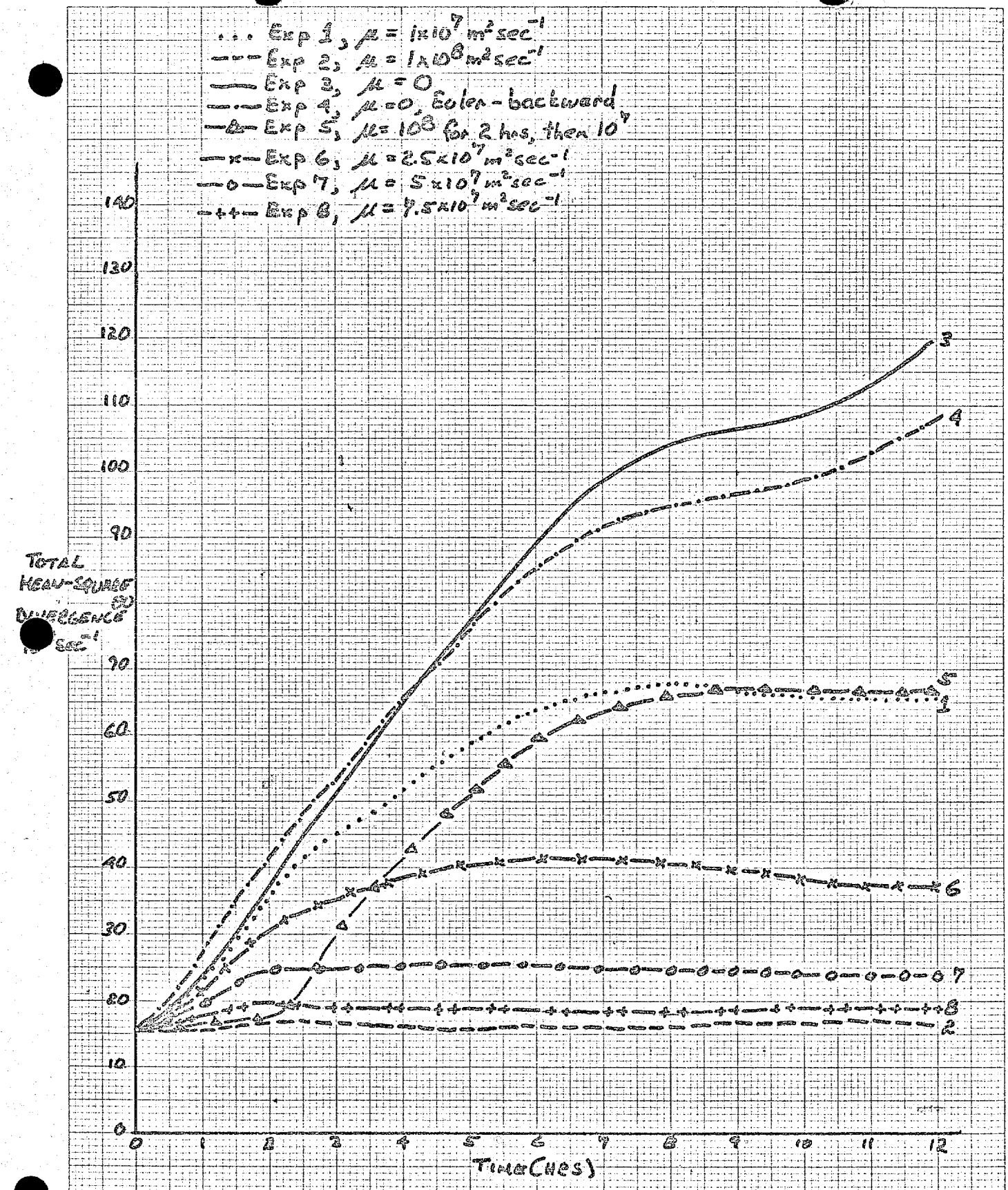
... Exp 1, $\mu = 1 \times 10^7$ m² sec⁻¹
--- Exp 2, $\mu = 1 \times 10^8$ m² sec⁻¹
—— Exp 3, $\mu = 0$
—·— Exp 4, $\mu = 0$, Euler-backward
—Δ— Exp 5, $\mu = 10^8$ for 2 hrs, then 10^7
—x— Exp 6, $\mu = 2.5 \times 10^7$ m² sec⁻¹
—o— Exp 7, $\mu = 5 \times 10^7$ m² sec⁻¹
—+— Exp 8, $\mu = 7.5 \times 10^7$ m² sec⁻¹
TOTAL MEAN-SQUARE DIVERGENCE (×10⁻¹² sec⁻¹)
0
10
20
30
40
50
60
70
80
90
100
110
120
130
140
0
1
2
3
4
5
6
7
8
9
10
11
12
TIME (HRS)
3
4
5
1
6
7
8
2

Figure 4

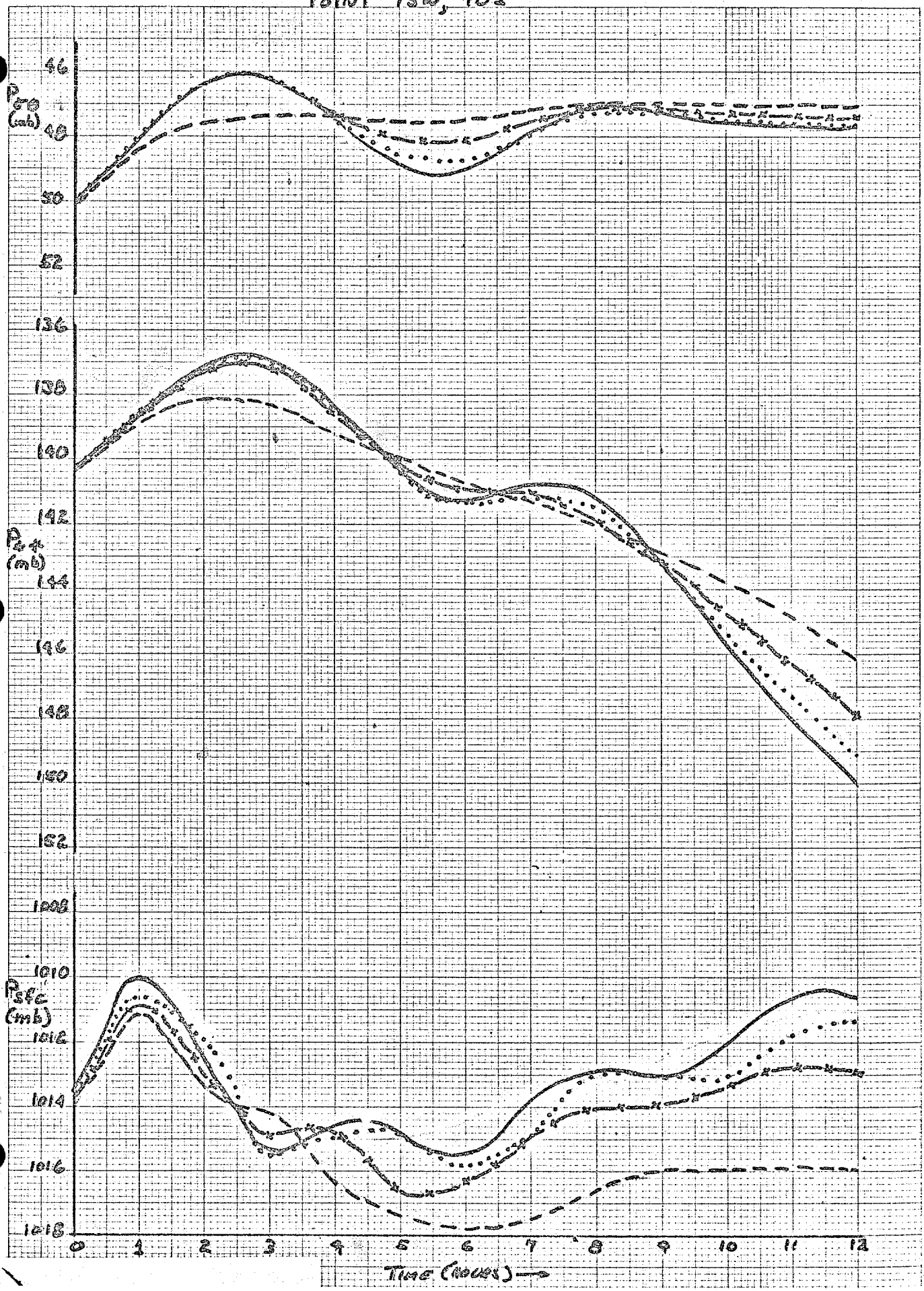
POINT 75W, 40S
P&O (mb)
46
48
50
52
P44 (mb)
136
138
140
142
144
146
148
150
152
P54C (mb)
1008
1010
1012
1014
1016
1018
0
1
2
3
4
5
6
7
8
9
10
11
12
TIME (HOURS)

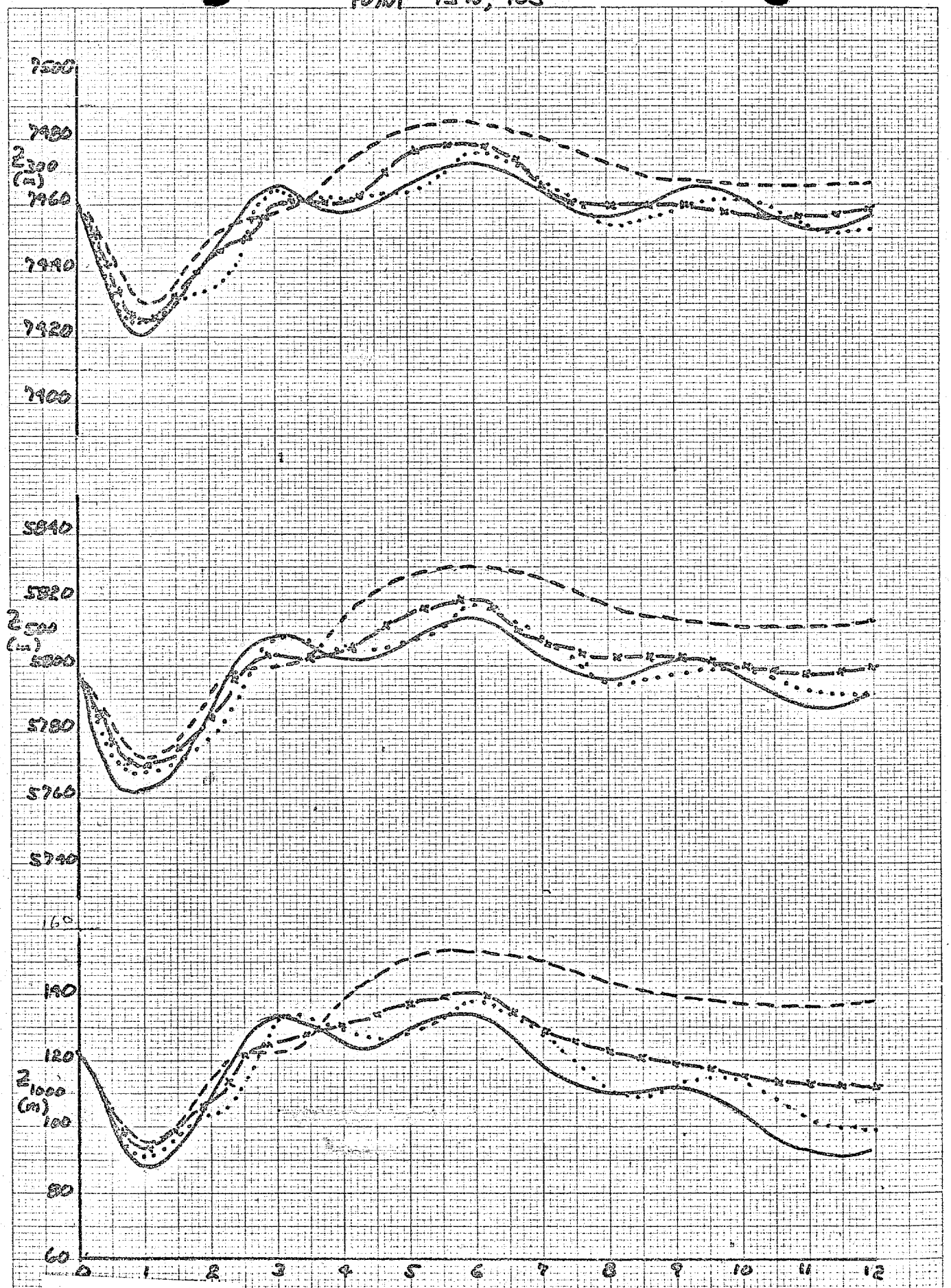
POINT 75W, 40S
7500
7480
Z500 (m)
7460
7440
7420
7400
5840
5820
Z500 (m)
5800
5780
5760
5740
160
140
120
Z1000 (m)
100
80
60
0
1
2
3
4
5
6
7
8
9
10
11
12
TIME (HOURS)

Figure 6

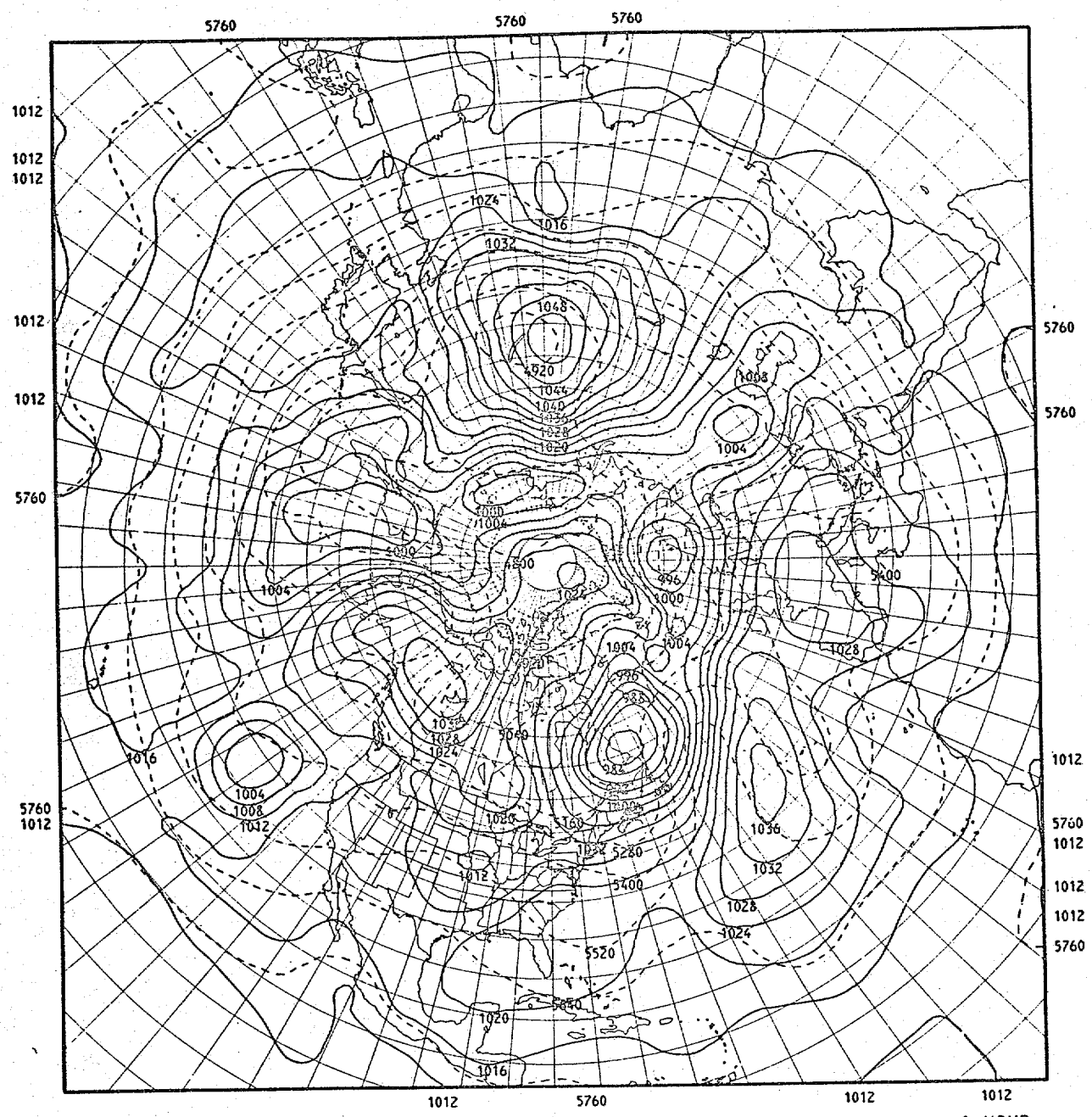

Figure 7

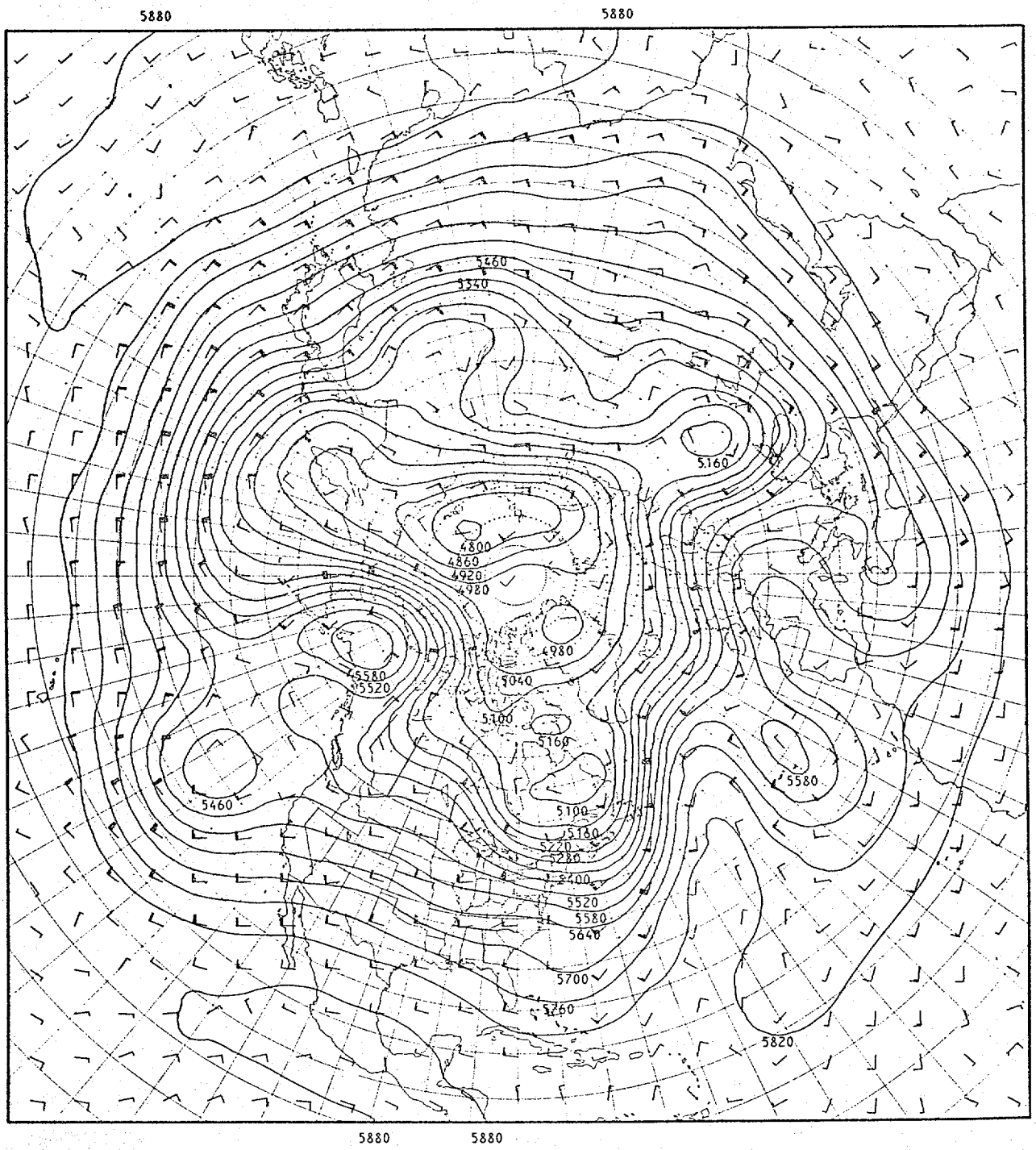

500 MB HEIGHTS AND VECTOR WINDS EXP. 3 2/ 5/73 0Z 0 HOUR

Figure 8

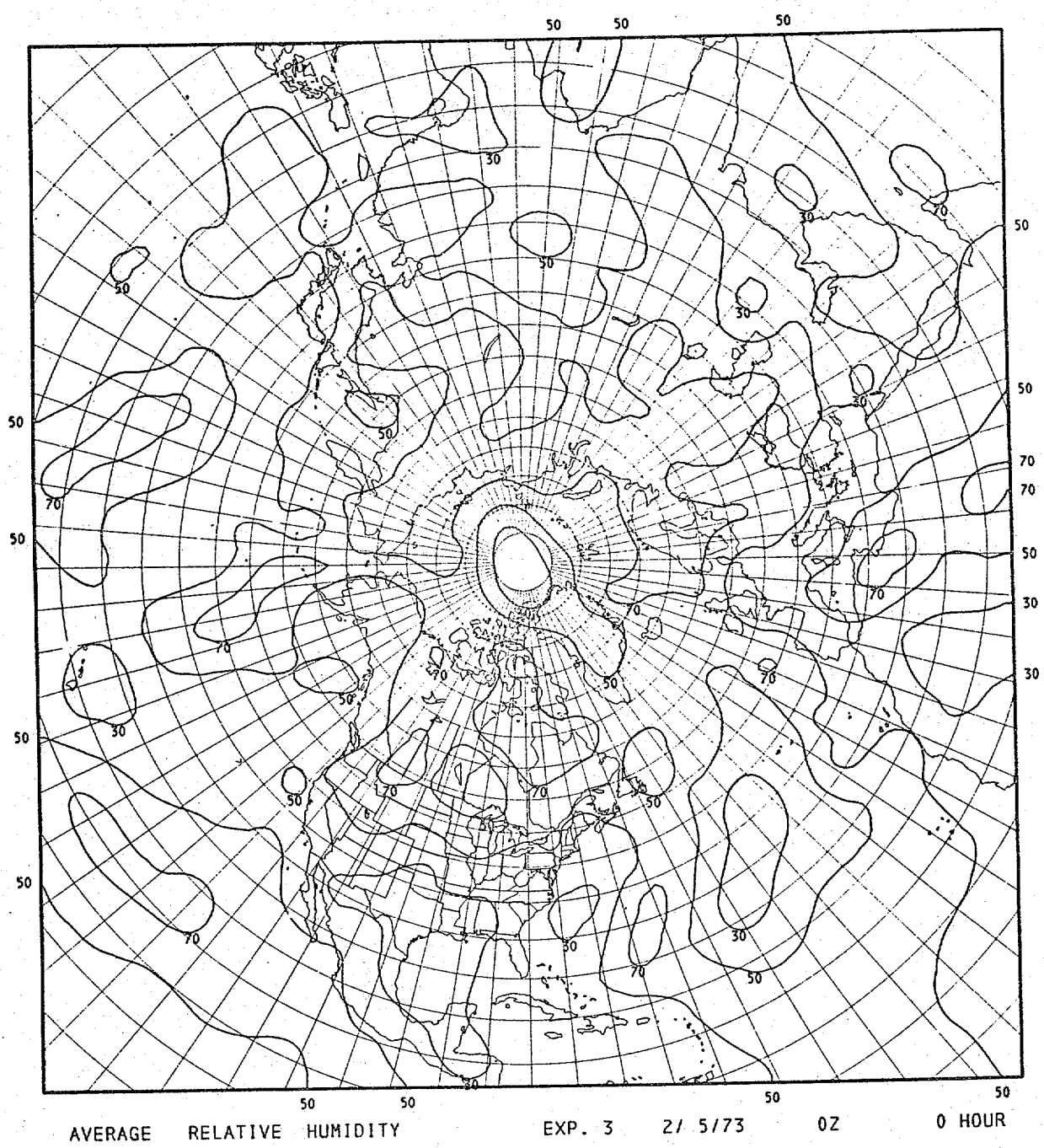

Figure 9

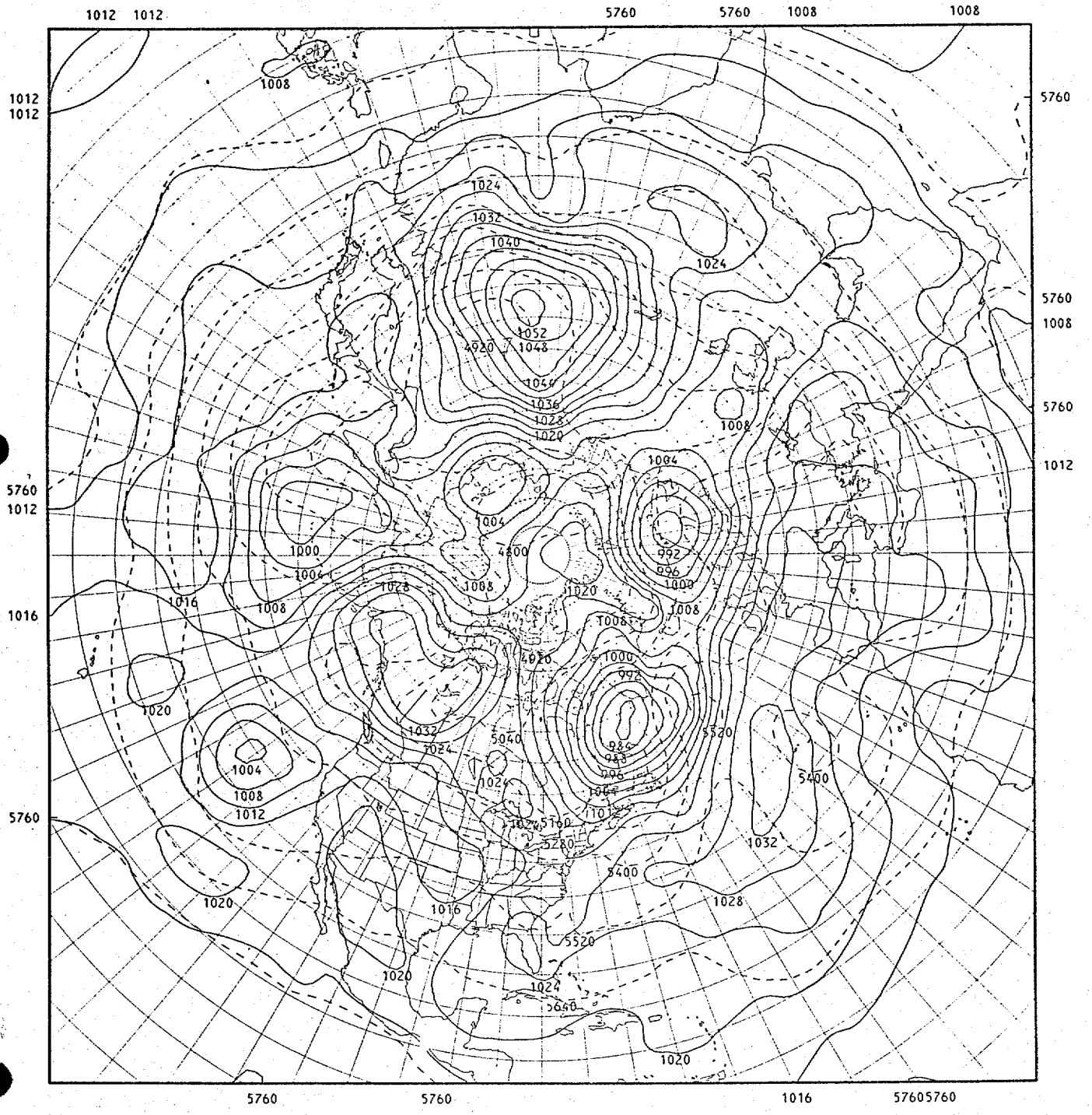
SEA LEVEL PRESS AND500-1000MB THICKNESS EXP. 3 2/ 5/73 0Z 12 HOUR

Figure 10

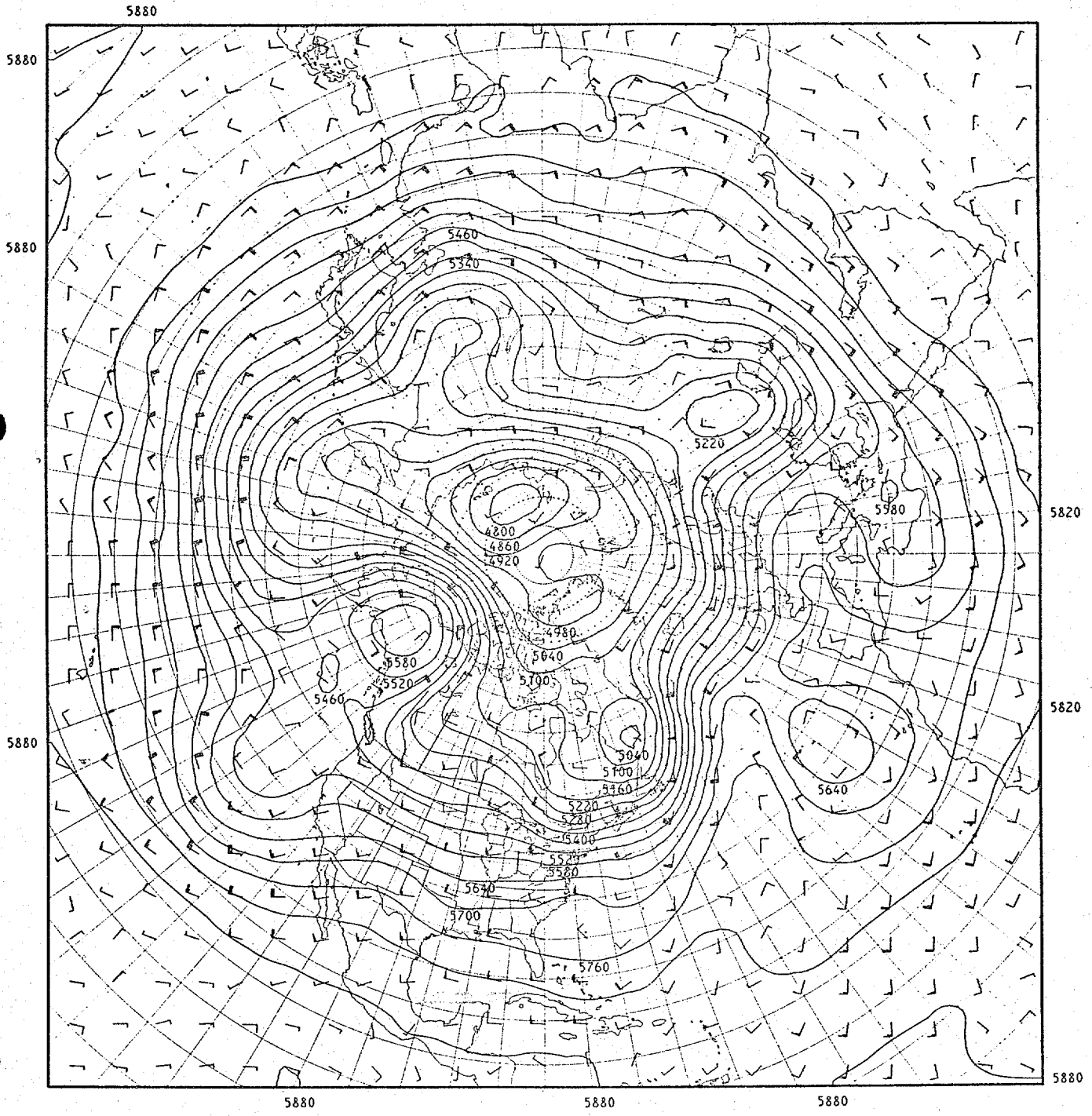
5880
5880
5880
5880
5820
5820
5880
5880
5880
5880
5460
5340
5220
5580
4800
4860
4920
4980
5040
5580
5520
5460
5700
5040
5100
5160
5220
5280
5400
5520
5580
5640
5700
5760
5640
500 MB HEIGHTS AND VECTOR WINDS EXP. 3 2/ 5/73 0Z 12 HOUR

Figure 11

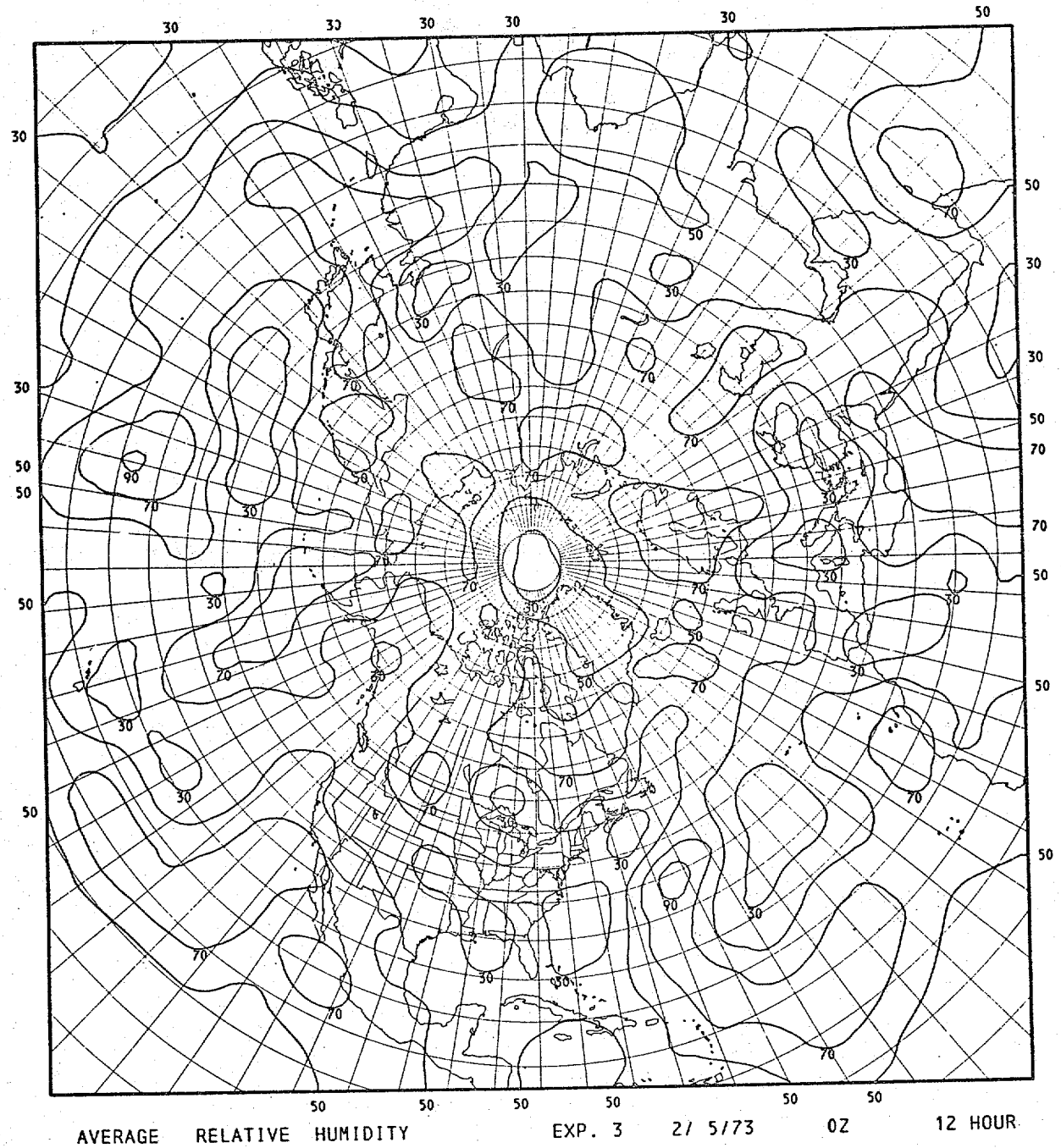

Figure 12

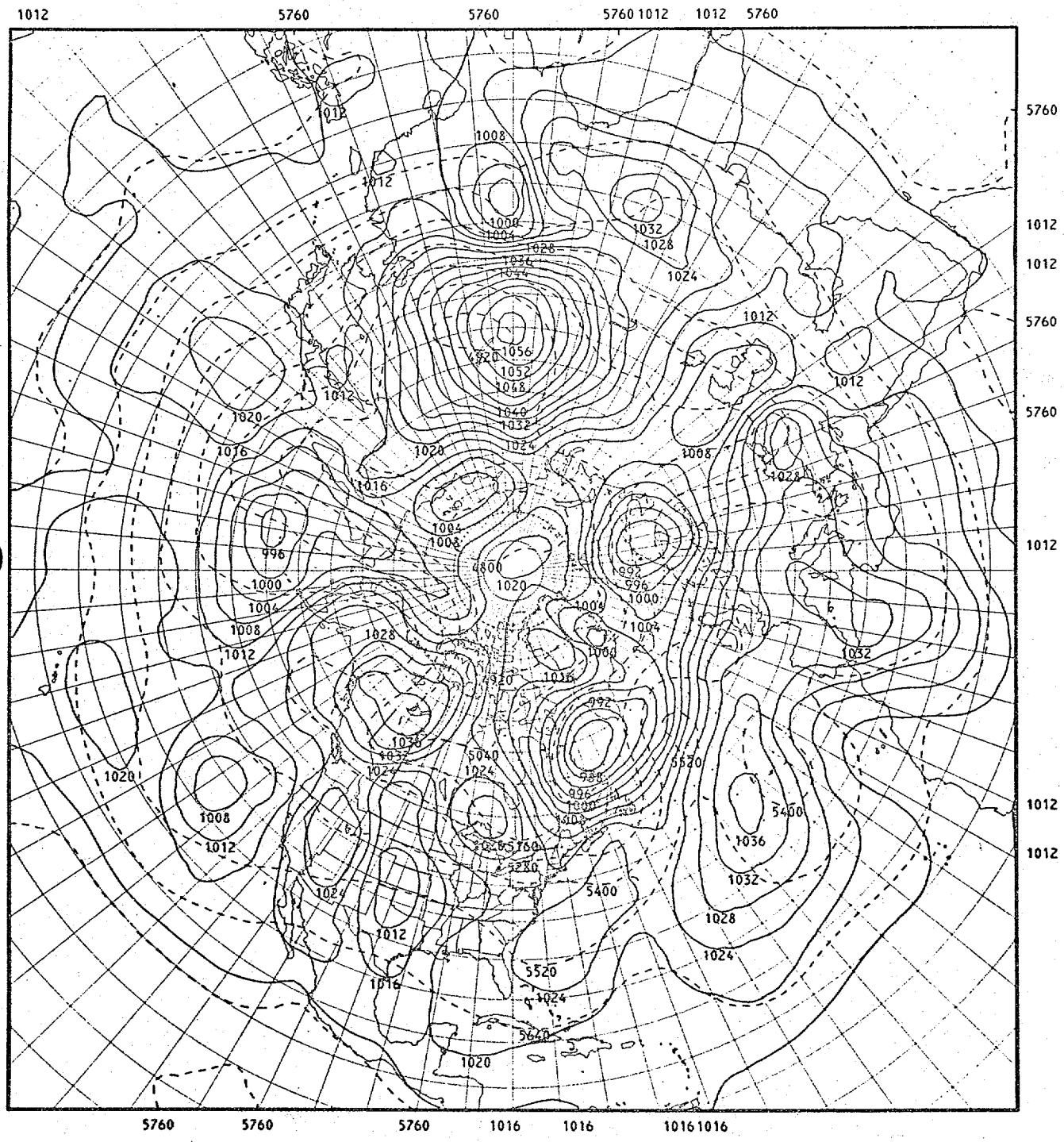
SEA LEVEL PRESS AND500-1000MB THICKNESS EXP 2 2/ 5/73 0Z 12 HOUR

Figure 13

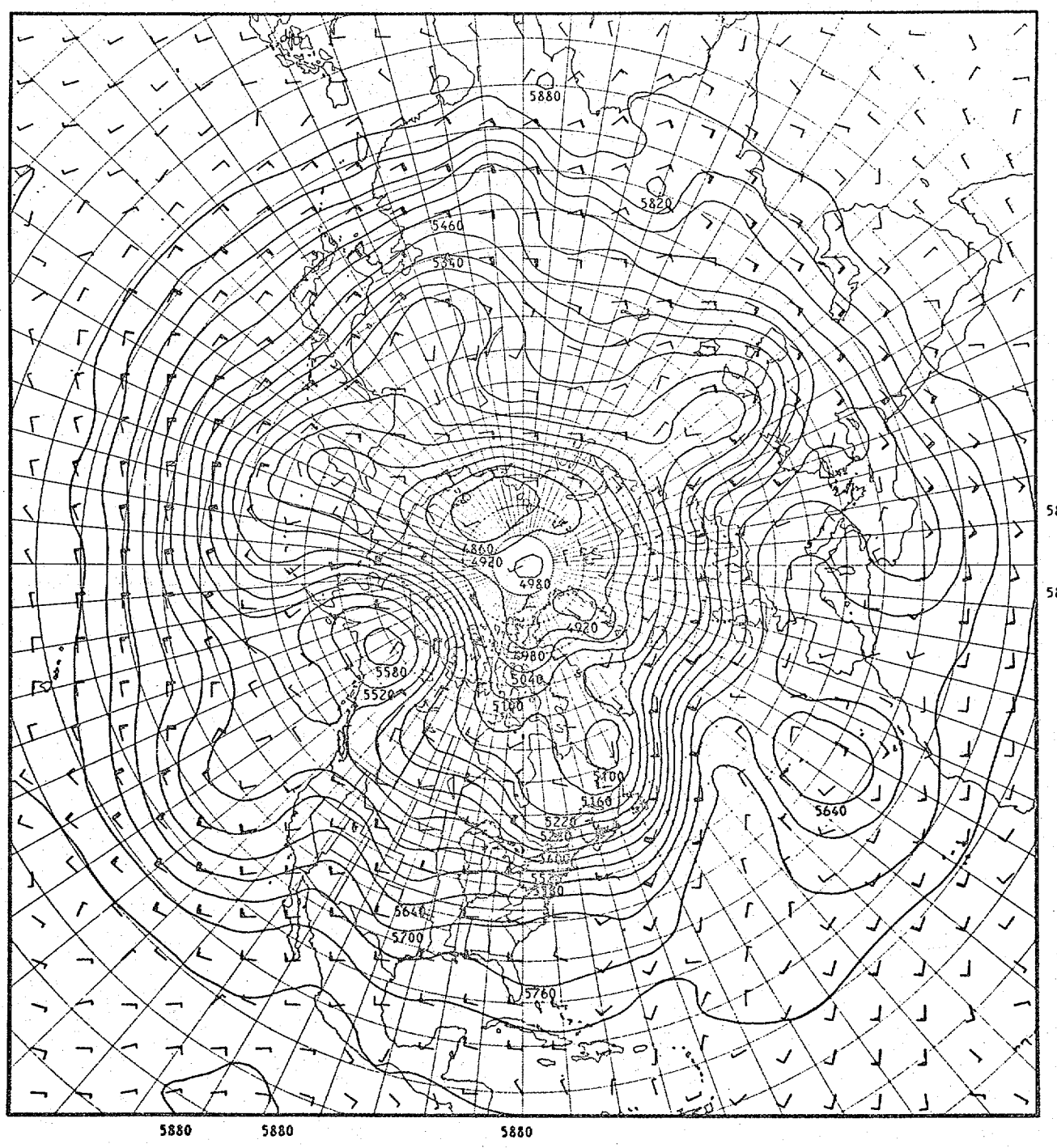
5880
5880
5880
5820
5820
5880
5880
5880
5880
5460
5540
5820
4860
4920
4980
4920
5040
5100
5580
5520
5100
5160
5220
5640
5700
5760
5640
5880
5880
5880
500 MB HEIGHTS AND VECTOR WINDS EXP 2 2/ 5/73 0Z 12 HOUR

Figure 14

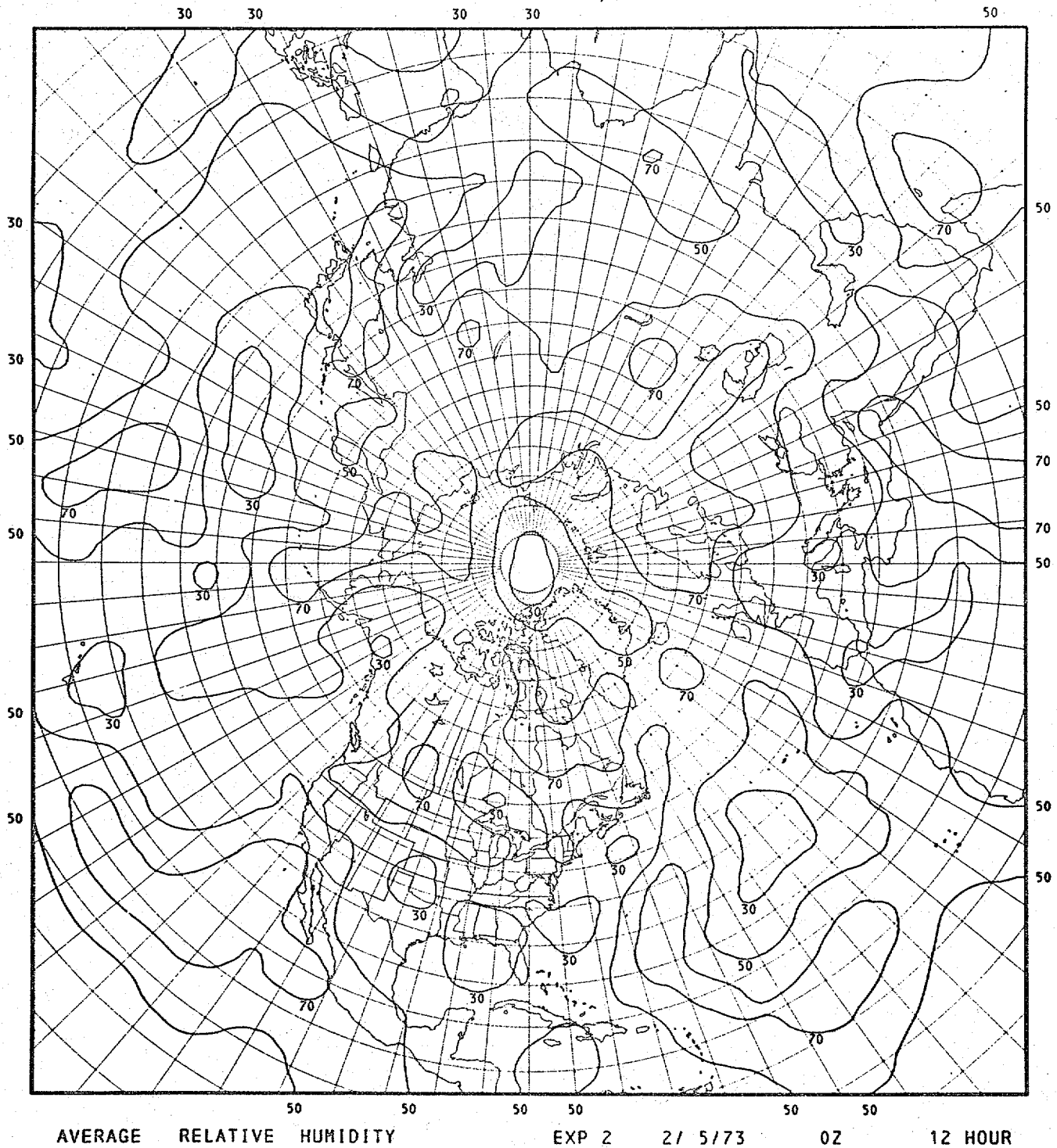

Figure 15

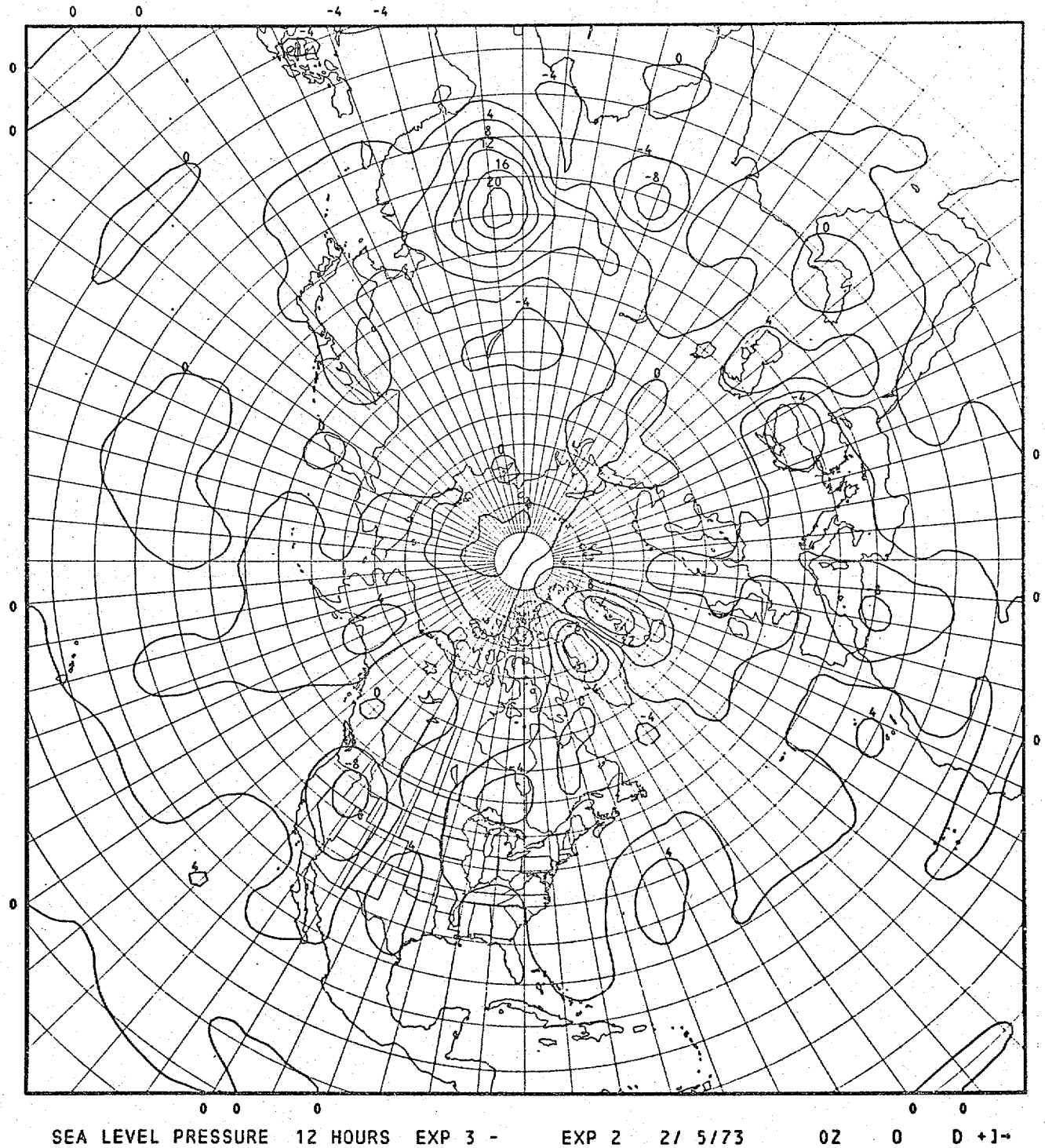

Figure 16

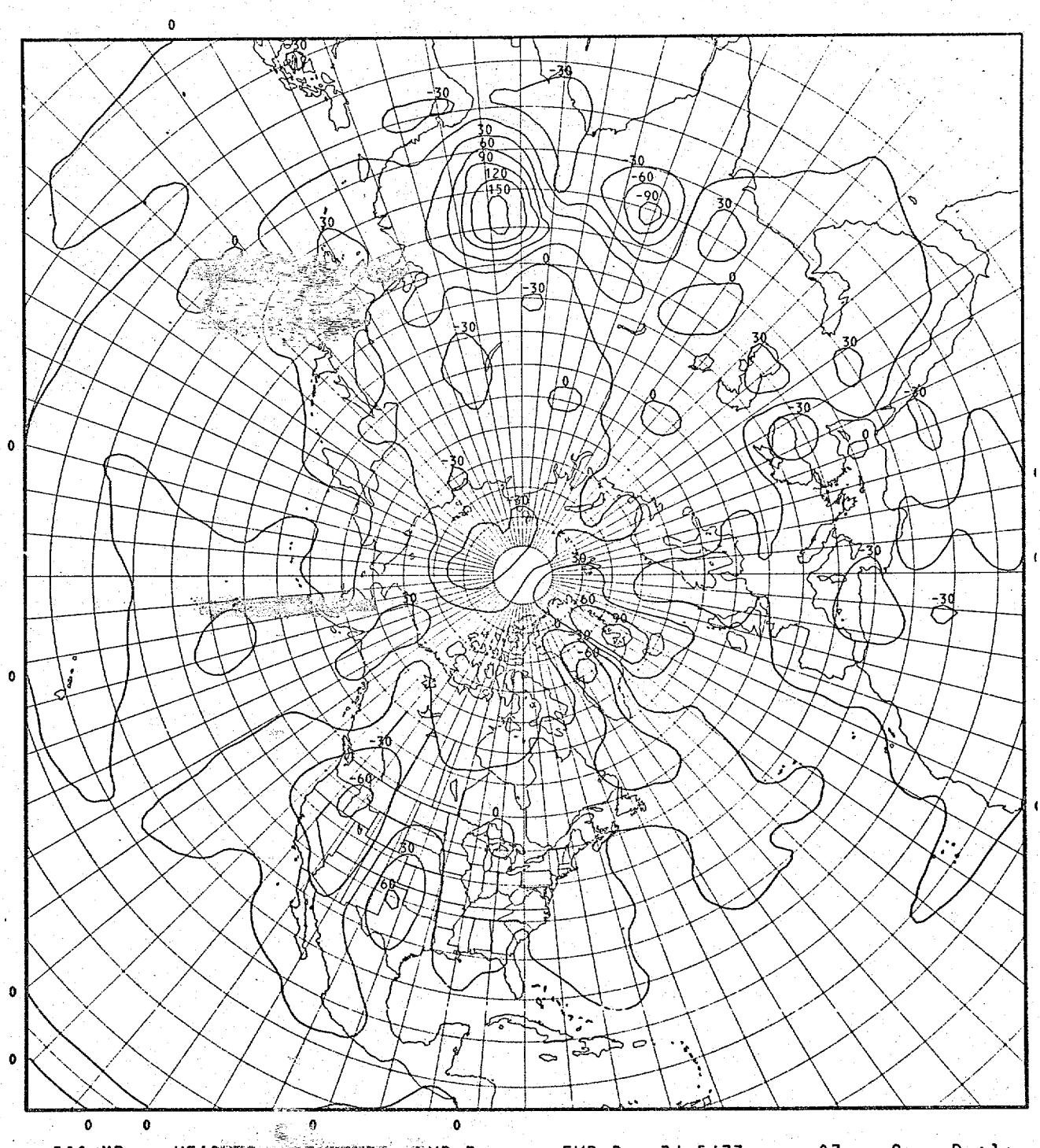

Figure 17

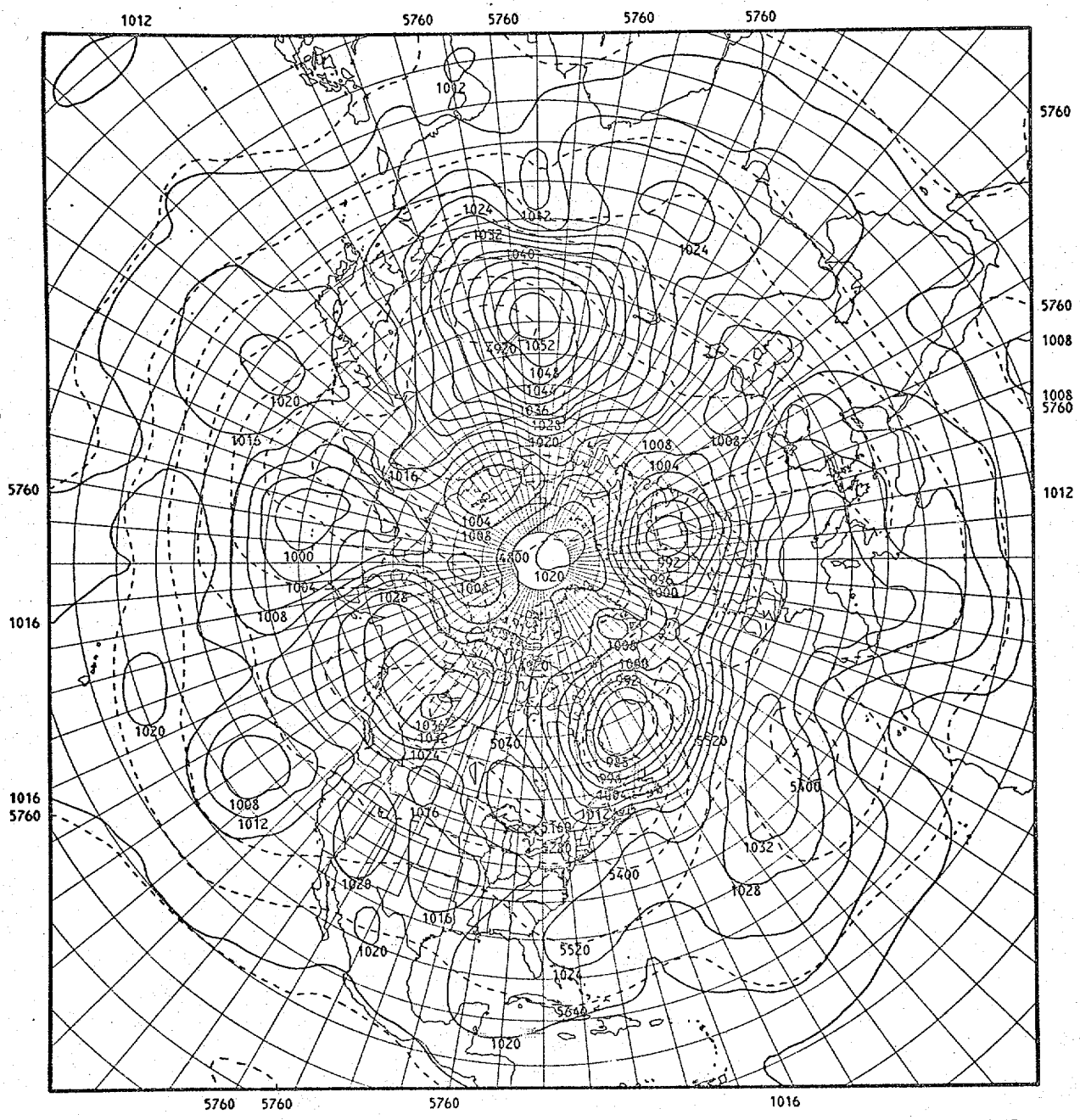
SEA LEVEL PRESS AND500-1000MB THICKNESS EXP 6 2/ 5/73 0Z 12 HOUR

Figure 18

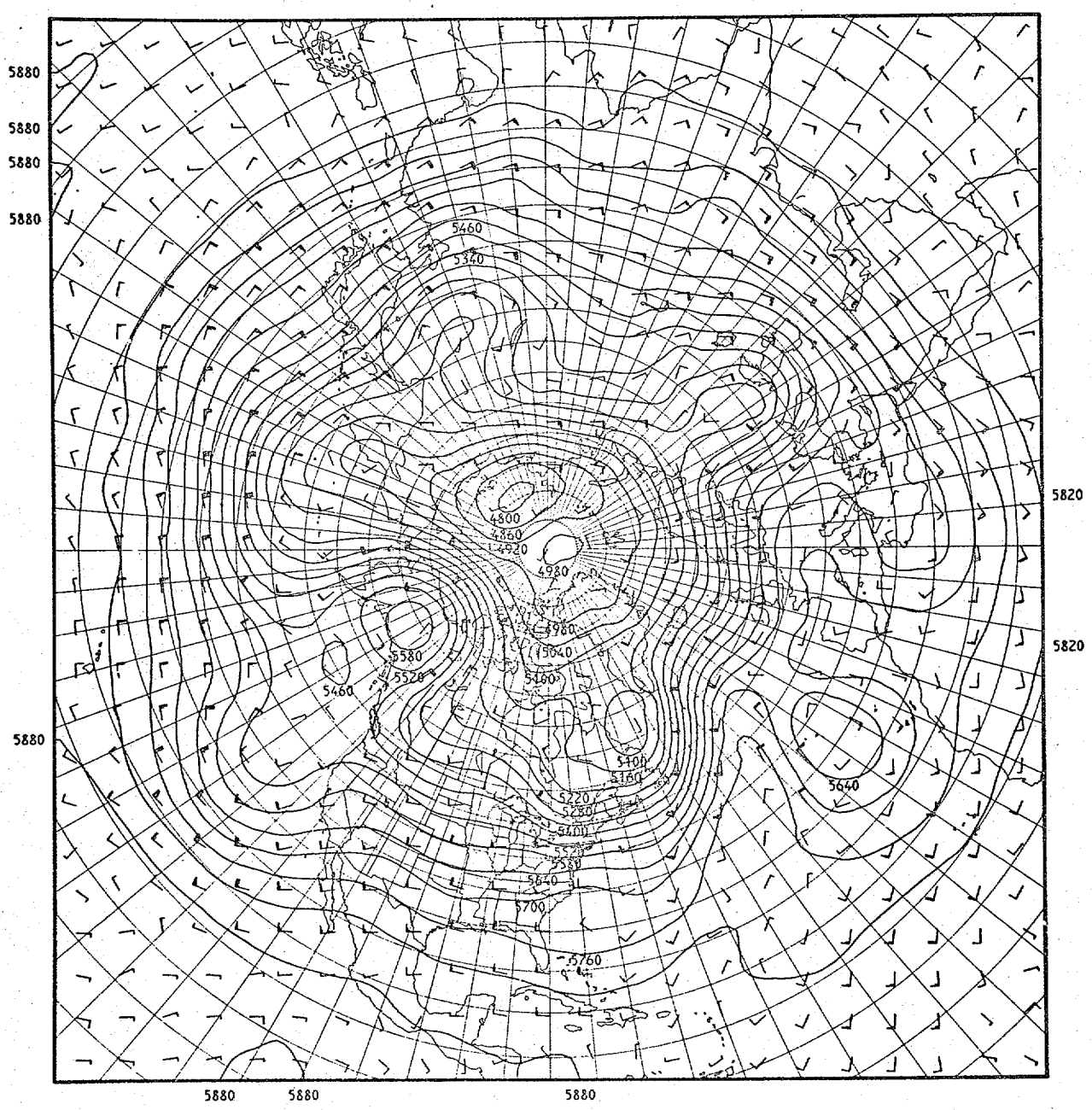
5880
5880
5880
5880
5820
5820
5880
5880
5880
5460
5340
4800
4860
4920
4980
5040
5160
5580
5520
5460
5100
5160
5220
5280
5400
5580
5640
5700
5760
5640
500 MB HEIGHTS AND VECTOR WINDS EXP 6 2/ 5/73 0Z 12 HOUR

Figure 19

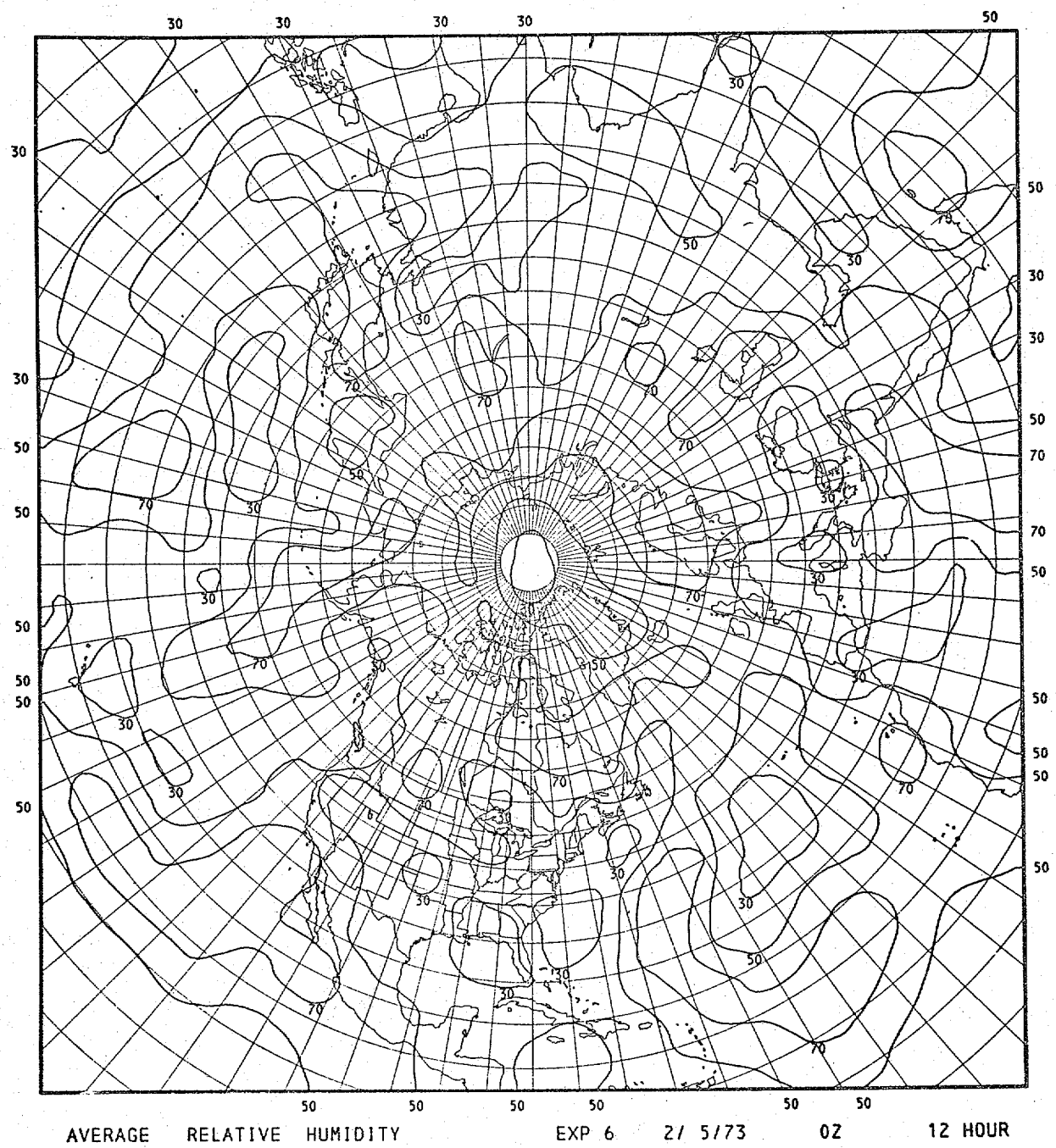

Figure 20

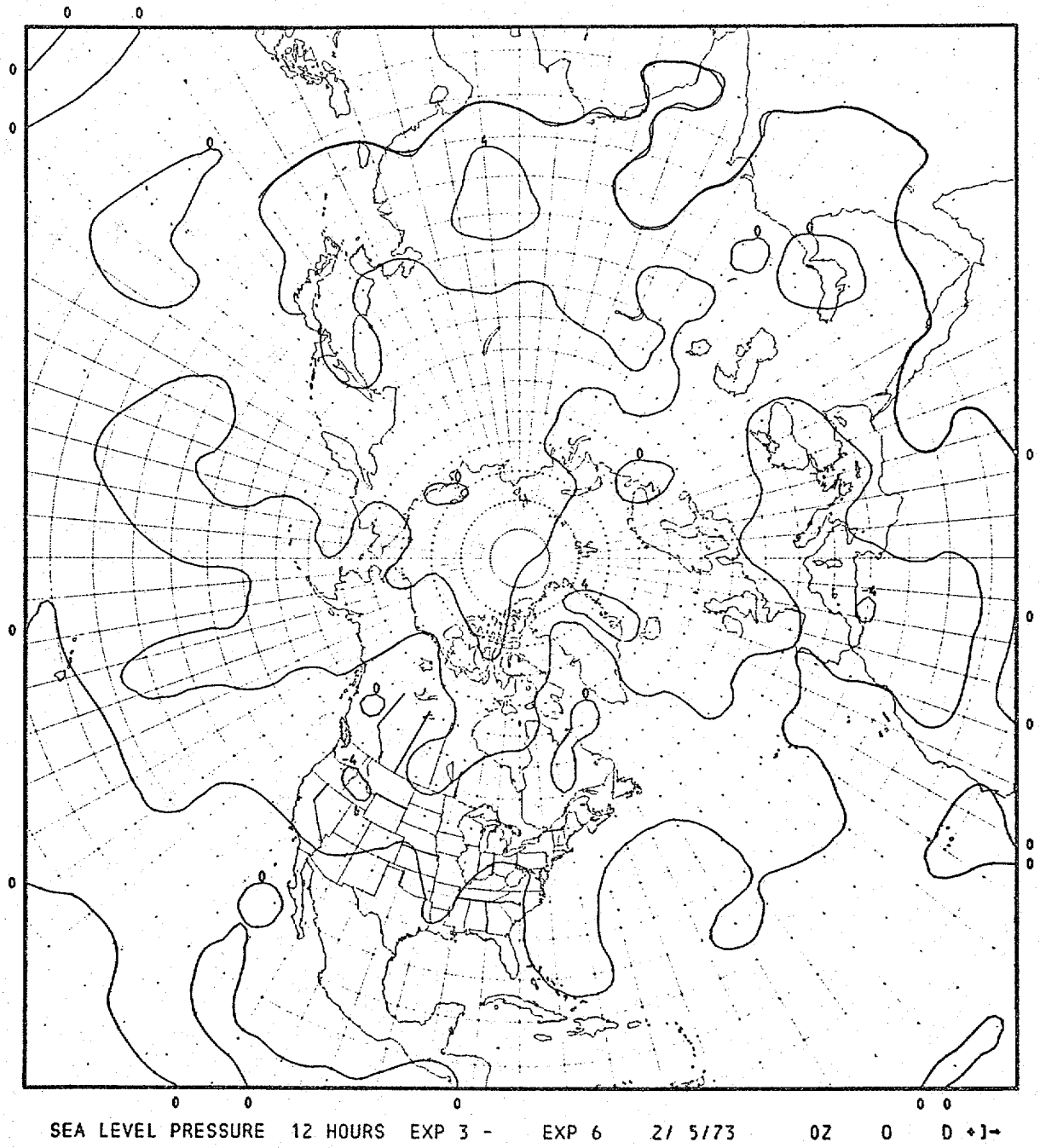

Figure 21

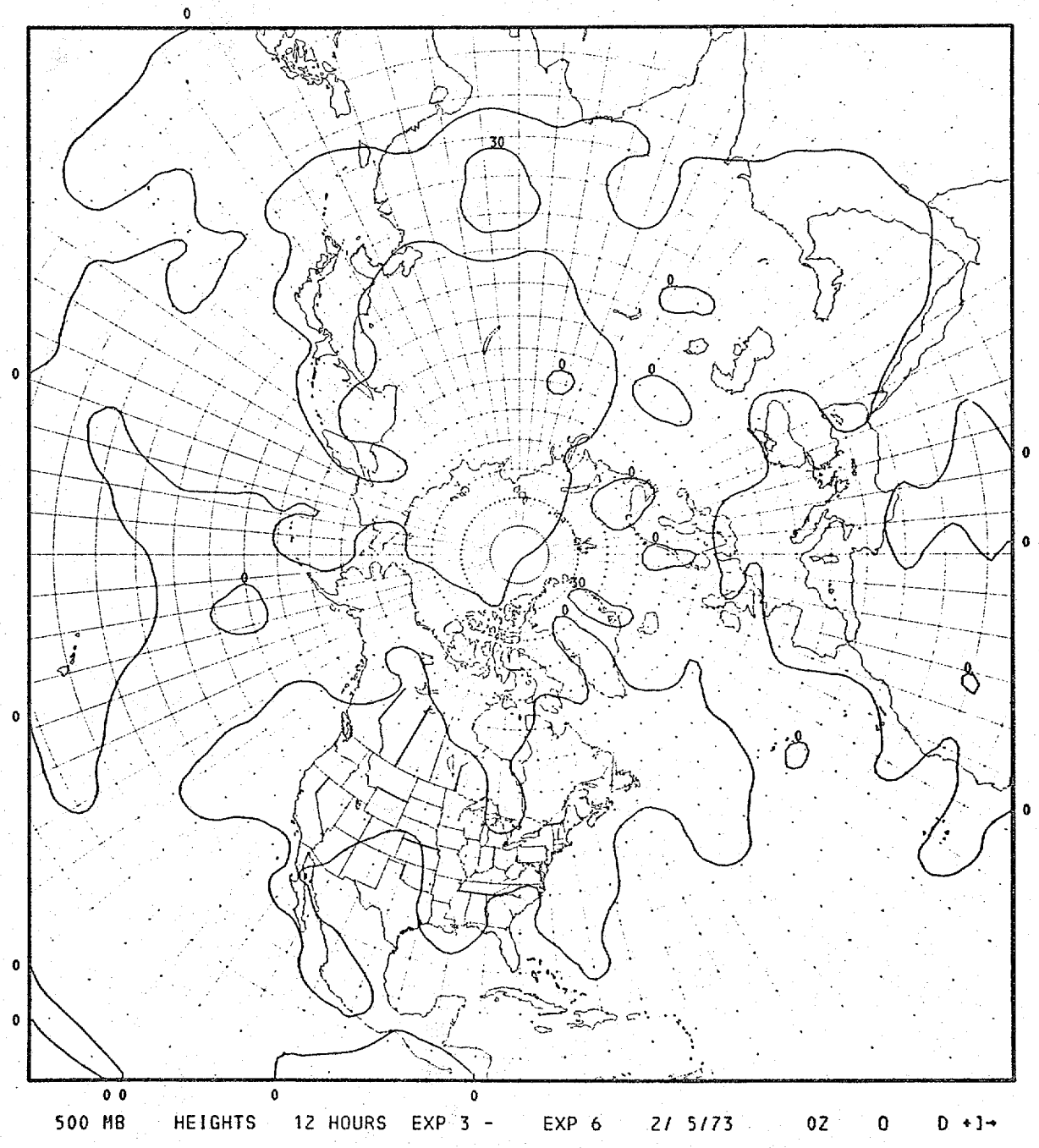

Figure 22